JOURNAL OF PHYSICAL ORGANIC CHEMISTRY
J. Phys. Org. Chem. 2001; **14:** 444–452
DOI:10.1002/poc.388

A non-topotactical thermal rearrangement without change of the macroscopic crystal shape

G. Kaupp,[1]* J. Schmeyers,[1] M. Kato,[2] K. Tanaka,[3] N. Harada[3] and F. Toda[4]

[1]Organische Chemie I, Universität Oldenburg, Postfach 2503, D-26111 Oldenburg, Germany
[2]Division of Material Science, Graduate School of Human Culture, Nara Women's University, Nara 630-8506, Japan
[3]Department of Applied Chemistry, Faculty of Engineering, Ehime University, Matsuyama, Ehime 790-8577, Japan
[4]Department of Chemistry, Faculty of Science, Okayama University of Science, Ridaicho 1-1, Okayama 700-0005, Japan

Received 10 December 2000; Revised 20 March 2001; Accepted 22 March 2001

epoc

ABSTRACT: The solid-state thermal transformation of *rac*-3,8-di(*tert*-butyl)-1,5,6,10-tetraphenyldeca-3,4,6,7-tetraene-1,9-diyne **(1)** into 4,5,9,10-tetraphenyltricyclo[6.2.0.0^{2,6}]deca-1,3,5,7,9-pentaene **(3)** was investigated by x-ray crystallography and atomic force microscopy (AFM) on two different faces. The enantiopure crystals of **1** that were picked from the conglomerate were monoclinic in the chiral space group *C*2 (No. 5) and were refined to an *R*-factor of 0.0375. The monolayers stack in a straight manner without displacement leaving (001) cleavage planes. The layered structure is seen in AFM traces at certain stages of the reaction. The overall shape of single crystals of **1** does not change even though they turn deeply blue–green at 140–150 °C. However, the initial roughness in the micrometer region is flattened out or thoroughly rearranged by long-range molecular movements giving phase rebuilding and phase transformation without detachment of the product from the parent crystal. Thus, the chemical reaction is limited to the surface region and to internal cracks of the crystal. A topotactical transformation is experimentally excluded and cannot be modelled at the given crystal structure. The chemical yield depends on the crystal size and is significant. The thermochrome **3** reverts to **1** but only in the outer surface region at anaerobic storage, whereas the known solid-state oxidations occur in air. The topographic differences of these processes were traced with AFM. The release of strain in the surface region is evidenced by anisotropic crack formation that initially follows the crystal packing of **1** and could be imaged and compared with an ordinary microscope after the thermal reversion or oxidation. Copyright © 2001 John Wiley & Sons, Ltd.
Additional material for this paper is available from the epoc website at http://www.wiley.com/epoc

KEYWORDS: atomic force microscopy; thermochrome; x-ray crystallography; crystal structure analysis; molecular migrations; solid-state reactions

INTRODUCTION

Organic reactions in crystals may proceed topotactically or non-topotactically. The former require that the overall geometric changes stay below 4% (Nakanishi criterion).[1] In such cases single crystal to single crystal conversions may occur.[2] The latter lead to molecular migrations and disintegration of the initial crystal.[2] Our previous observation that heating of the crystalline diallene **1** to 140 °C gives the solid thermochrome benzodicyclobutadiene **3**[3,4] (Scheme 1) without change in the overall crystal shape[5] was at odds with these findings because the molecular shapes of **1** and **3**[6] have nothing in common. We therefore performed an x-ray study of **1** and an atomic force microscopic (AFM) study of its thermal conversion and report on unexpected results.

RESULTS AND DISCUSSION

X-ray structure determination

The crystal structure of **1** was solved by direct methods using a Rigaku AFC7R diffractometer and refined to an *R*-factor of 0.0375. The molecular structure and numbering of **1** are given in Fig. 1 with important bond lengths and ellipsoid representation (50%).

Enantiopure monoclinic crystals of the chiral space group *C*2 (No. 5) were selected from the conglomerate of racemic **1** with $a = 24.425(3)$, $b = 7.431(2)$, $c = 9.456(2)$, $\beta = 98.50(2)$ and two formula units in the unit cell with a

**Correspondence to:* G. Kaupp, Organische Chemie I, Universität Oldenburg, Postfach 2503, D-26111 Oldenburg, Germany.
Email: kaupp@kaupp.chemie.uni-oldenburg.de

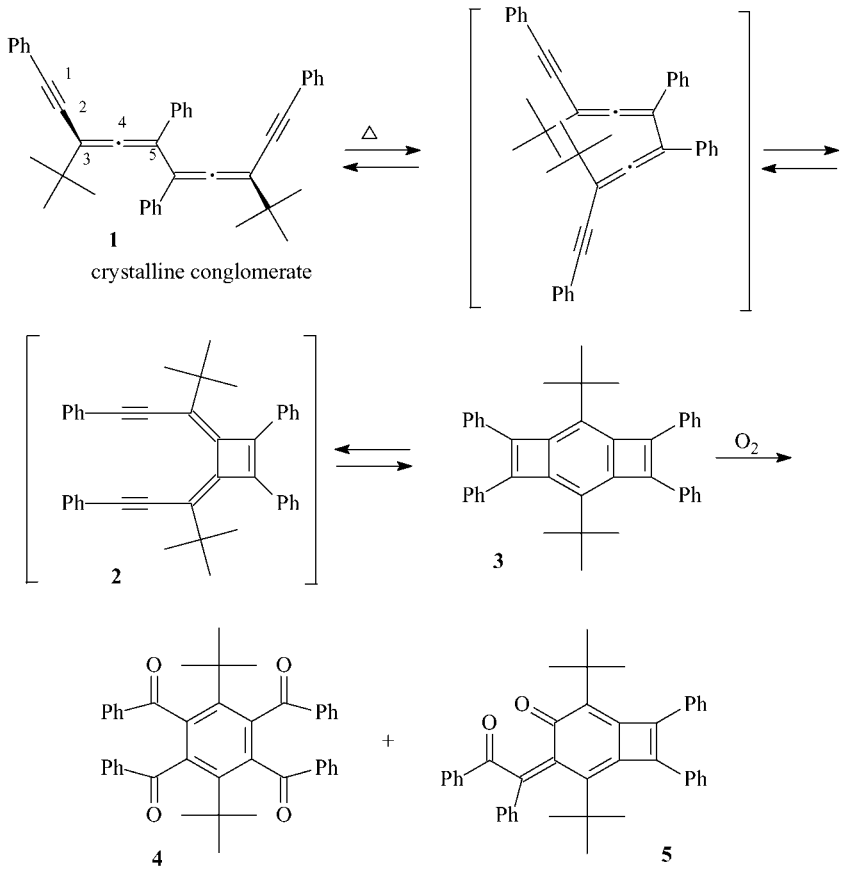

Scheme 1. Thermal transformation of **1** into **3** with the presumed intermediates and the solid-state oxidation with air

calculated density of 1.062 g cm^{-3}. The prismatic crystal forms exhibit prominent {001} (rhombus) and {100} faces (rectangles with skew {110} faces on top and bottom). Full data, including structure factors, are listed in the epoc material at http://www.wiley.com/epoc.

Thermal treatment of the crystals of 1

Heating of single crystals, micronized powders and KBr pellets (mortar) of **1** for 2 or 4 h at 140–150 °C created the blue–green color of **3**. If the heating was performed under

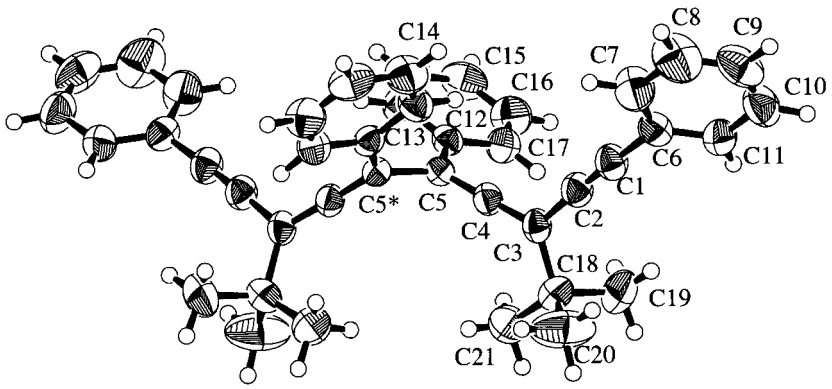

Figure 1. Molecular structure of **1**. The molecule has crystallographic two fold symmetry through the center of the C5—C5* bond. Selected bond lengths (Å) and angles (°): C1—C2 = 1.192(4), C1—C6 = 1.443(4), C2—C3 = 1.449(4), C3—C4 = 1.302(4), C3—C18 = 1.531(4), C4—C5 = 1.319(3), C5—C5* = 1.523(5), C5—C12 = 1.486(4), C2—C1—C6 = 178.2(3), C1—C2—C3 = 177.4(3), C2—C3—C4 = 118.9(3), C3—C4—C5 = 176,6(3), C4—C5—C5* = 118.1(3)

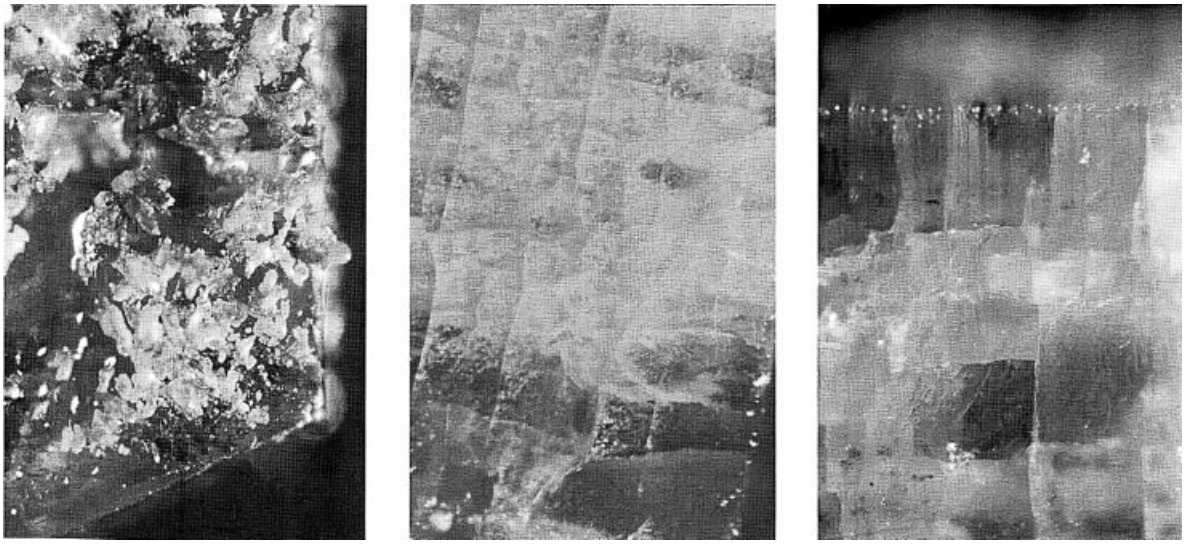

Figure 2. Micrographs of thermally treated single crystals of **1** at 100-fold magnification. Left, heated under vacuum, on (001) after 12 days rest in a vacuum; middle, heated in air on (001) after 6 days rest in air; right, heated in air on (100) after 3 days rest in air. The length of the *x*-axis of the images corresponds to 900 μm.

vacuum the yield was 17–25, 20–28 and 50% (the pellet must be prepared under Ar or N_2), respectively. The rest of the material was **1**. The ratio of **1** and **3** was judged from the intensities of the out-of-plane deformation vibrations of **1** (692 and 759 cm^{-1}) and **3** (713 and 741 cm^{-1}). If similar heating was carried out in air the single crystals of **1** gave 8–10% of **3**, besides the oxidation products **4** and **5**,[5,7] and much unreacted **1**. If the green pellets or the crystals of pure **3** were stored under Ar or N_2 they did not change their color for months at room temperature. The crystals' deep blue–green color faded to yellow at the surface in the course of several

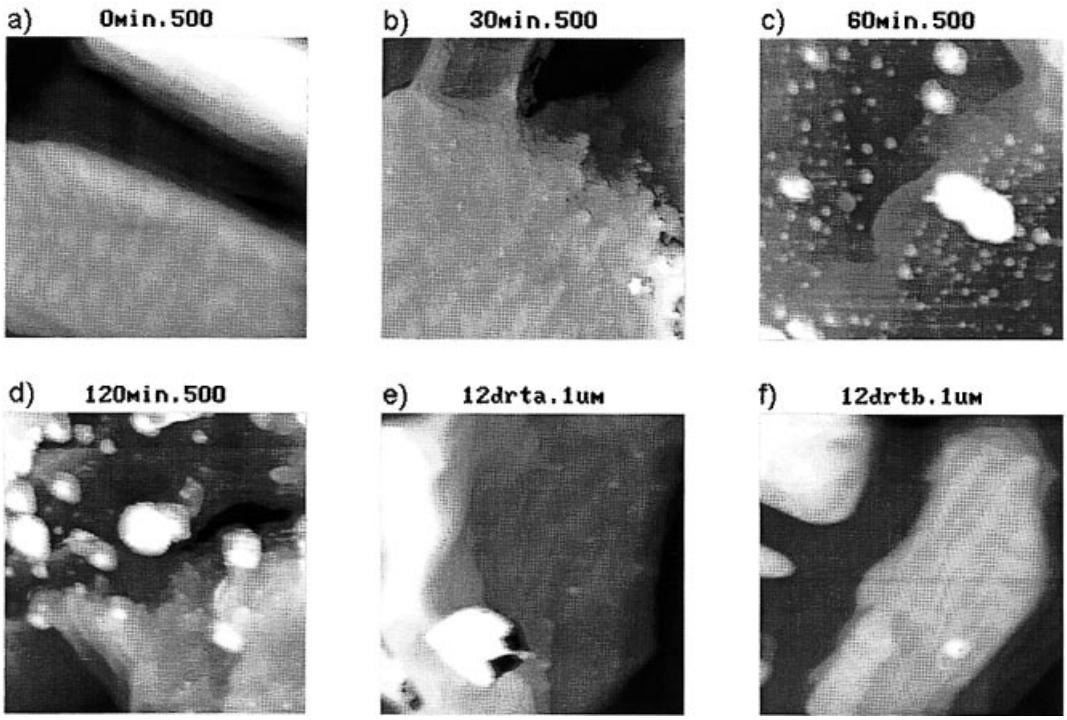

Figure 3. Typical 9.5 μm AFM topographies of a crystal of **1** on (001) (rhombus) before and after heating at 140 °C in a vacuum; heating times (the 12drt indicate rest at room temperature in a vacuum, when yellow material grew on it, and AFM measurement at different sites a and b) and *Z*-scales in nm (unless stated as μm) are as indicated before and after the dots. High- and low-resolution VRML images of (a)–(f) are available at the epoc website at http://www.wiley.com/epoc

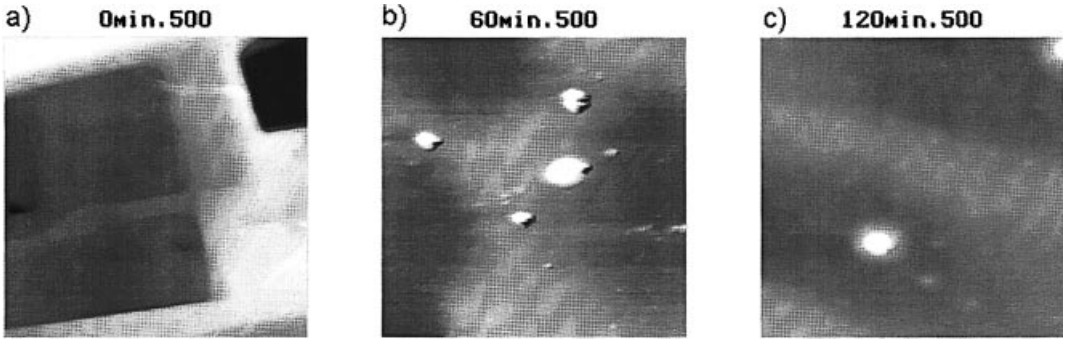

Figure 4. Typical 9.5 μm AFM topographies of a crystal of **1** on (100) (rectangle) before and after heating at 140 °C in a vacuum; heating times and *Z*-scale in nm are as indicated before and after the dot. High- and low-resolution VRML images of (a)–(c) are available at the epoc website at http://www.wiley.com/epoc

days both in vacuum and in air. The shape of the crystals did not change visibly,[5] but microscopic inspection at 100-fold magnification revealed marked microscopic changes (Fig. 2). Clearly, sharp edges remained at the rhombic and rectangular faces despite the chemical reactions. In the left image in Fig. 2 irregular yellow crystallites grew on the still green crystal and this color persisted for several weeks. The yellow material consists of **1** (singlet at 1.22 ppm in $CDCl_3$). It could by easily removed. The initial roughness of that face was of profoundly different character.

Heating of **1** in air for 5, 30, 60 and 120 min with interrupts for AFM measurements (see below) and then resting in air led to totally different results. The initially rough surface (heights and depths of about 1 μm) became very smooth with initially three microscopic trenches on (001) along the long crystal edge. The trenches that are seen in the middle and right images of Fig. 2 developed gradually after 1–6 and 3 days in air when the color changed to yellow with residual green spots under the surface. The trenches in the middle image on (001) go along [010] and [100] and those in the right image on

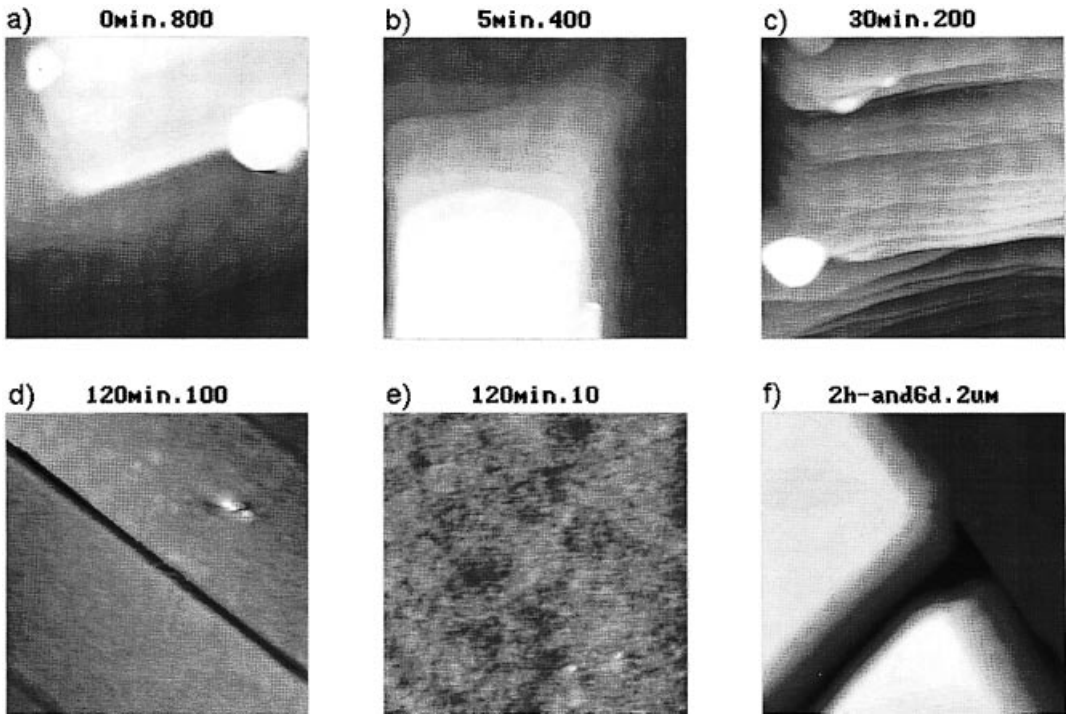

Figure 5. Typical 7.5 μm AFM topographies of a crystal of **1** on (001) in various orientations for the best view before and after heating in air at 140 °C; heating times (6d indicates rest at room temperature in air) and *Z*-scales in nm (unless stated as μm) are as indicated before and after the dots. High- and low-resolution VRML images of (a)–(f) are available at the epoc website at http://www.wiley.com/epoc

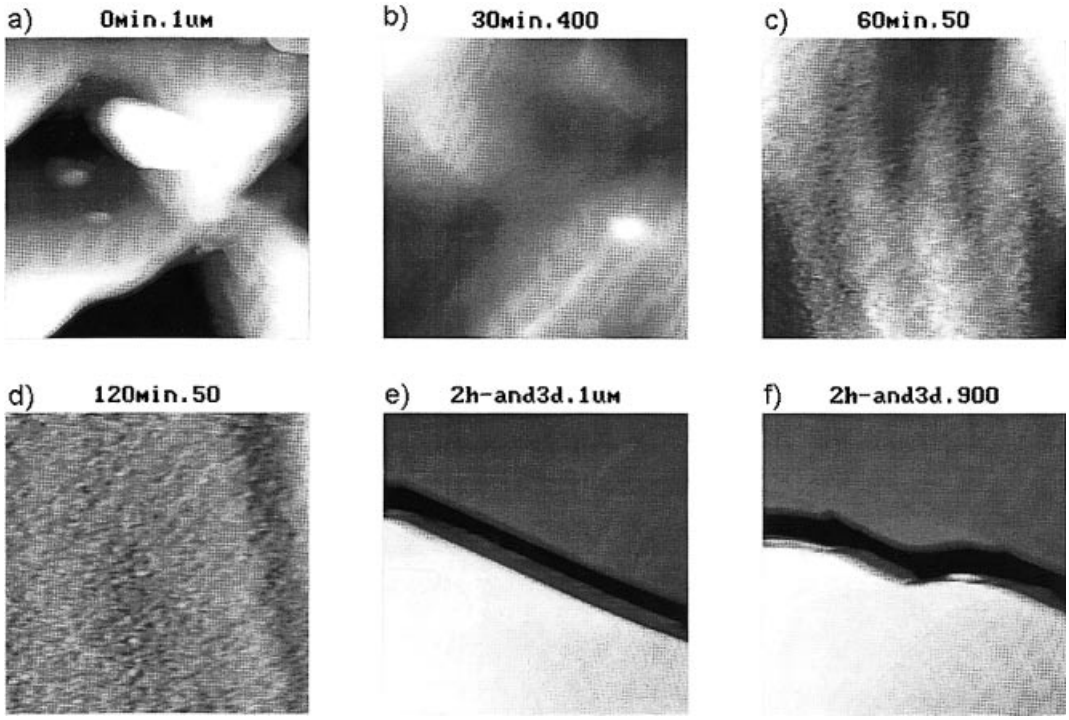

Figure 6. Typical 9.1 μm AFM topographies of a crystal of **1** on (100) before and after heating in air at 140 °C at different times and sites in various orientations for the best view; heating times (3d were at ambient temperature in air) and *Z*-scales in nm (unless stated as μm) are as indicated before and after the dots. High- and low-resolution VRML images of (a)–(f) are available at the epoc website at http://www.wiley.com/epoc

(100) along [010] and [001]. Therefore, Fig. 2 shows that in the presence of oxygen roughly orthogonal cracks in three directions cut numerous small crystals out of the mother crystal but these stick together on the surface. Such behavior was enhanced further if the heating to 140 °C was not interrupted but applied in one step: the cracks in all three directions appeared immediately at roughly the frequency of Fig. 2 and more distinct. Hence the change in color is not related to the crack formation. The chemical result was studied after 1 month's rest in air, when all residual green **3** had disappeared. ^{1}H NMR analysis indicated the presence of **1** with 8% of **4** and 4% of **5** and a singlet peak of unknown origin at 1.55 ppm. If the micronized material that had largely faded in vacuum was analyzed, only **1** was detected in the ^{1}H NMR spectrum besides the oxidation products of residual **3** that form upon dissolution in $CDCl_3$: **4, 5** and the epoxide precursor[7] to **4**. Therefore, we have a thermochrome in the solid state. However, the left image of Fig. 2 indicates that the reversion of **3** to **1** occurs primarily at the surface and thus the thermochromic behavior may profit from the cracks in the crystal that provide additional surface. Similarly, the higher yield of **3** upon heating of ground **1** in KBr pellets is explained by the higher surface area for the product formation. However, if the surface is excessively enlarged by using micronized powder of **1**, there is no marked increase in the yield as compared with that found in the single crystal. This observation shows that not much **3** survives as its transformation into **1** occurs primarily at the surface region and not in the bulk. A submicroscopic AFM study revealed further mechanistic details for the understanding of the rather involved behavior.

AFM investigation

The starting crystals of enantiopure **1** (*C*2) (conglomerate from acetone) were very rough on their most prominent (001) and (100) faces [Figs 3(a), 4(a), 5(a) and 6(a)]. They were measured by AFM at various sites to establish the roughness everywhere. They were then heated at 140 °C for 5, 30, 60 and 120 min both in vacuum and in air with intermittent measurement of the surface changes by AFM. It turned out that the rough surface on (001) changed considerably at the submicroscopic level if the heating was performed in a vacuum. The initially smooth large blocks, that extend at an angle of 30° to the long crystal axis [010], became structured with floes and later with islands (300–450 nm high) and smaller volcano-like hills (up to 110 nm high). Figure 3 indicates that the initial surface was completely changed with the straight edges becoming irregular, even though the macroscopic shape of the crystal was retained. A rather drastic change

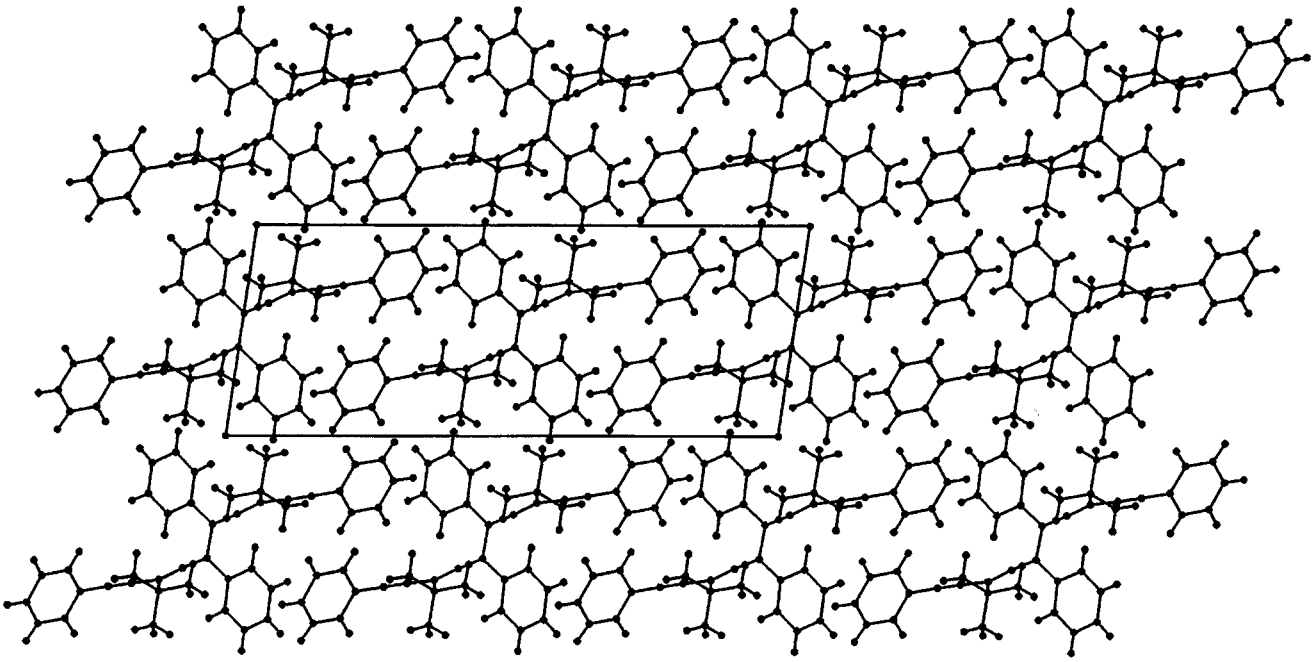

Figure 7. Stereoscopic packing of the crystals of **1** on (010) showing the (001) cleavage planes. The packing range was chosen to include three layers of molecules along [010] in order to show both the interlocked monolayers of the extended molecules and their straight stacking along [010]

of the surface is seen in images (e) and (f) after 12 days rest in a vacuum when the dark green color at the surface had essentially turned to yellow owing to re-formation of **1**. Both islands and terrace-like structures are seen after that transformation in crystal regions of lower roughness (cf. Fig. 2, left image). Anyhow, the material anisotropically migrates over long distances above the crystal surface upon the thermal reactions and we have thermochromism at the surface. As expected, the behavior is different on (100) of **1** (Fig. 4). The initially rectangular basins are completely lost and the surface becomes fairly smooth with some islands on it. Clearly, a levelling of the surface prevails.

These experimental findings indicate long-range anisotropic movements of molecules upon thermal isomerizations of **1** via **2** to **3**[6] and of **3** to **1**. They exclude topotactic reactions even though the macroscopic crystal shape is retained. It is known that crystalline **3** oxidizes slowly at room temperature in air to give 13% of the tetrabenzoylbenzene **4** and 50% of the quinomethide **5**.[5,7] It was of interest to study that reaction by heating **1** in air and storing the green crystal in air. Interestingly, but not unexpectedly, the AFM results from aerobic heating were totally different from those from anaerobic heating (Figs 5 and 6). It turned out, that the surfaces became increasingly flatter the longer the heating period, while the crystal turned green owing to formation of **3** and some **4** and **5** (IR evidence).

The irregular surface shape in Fig. 5(a) became flatter and structured after 5 min (b) and 30 min heating (c). After 120 min heating sporadic trenches parallel to the long crystal axis are seen (d), but the now formed plane is very flat in the areas without trenches (e) (roughness: $R_{ms} = 0.36$ nm). If the deep green sample was left under ambient conditions for 3 or 6 days it developed a yellow–greenish color and steep slopes (typically 30°, some >55°) were found at selected sites at dislocations (f) that have heights in the range of 1 μm and run along the long crystal edges [010] and more rarely at right-angles to it.

A different behavior was found on (100) of **1**. The initially rough surface [Fig. 6(a)] became flat more directly [Fig. 6(b)–(d)] and high dislocations with steep (>55°) trenches along [010] were found upon standing for 3 days in air on the now more yellow crystal surface [Fig. 6(e) and (f)]. Interestingly, the sharp edges may be straight or wavy and there was a further decrease in the roughness R_{ms} from 1.44 [Fig. 6(d), left] to 0.3–0.4 nm on the plateaux in Fig. 6(e) and (f).

Mechanistic discussion

Solid-state mechanism. The microscopic and submicroscopic investigations of the thermally transformed crystals of **1**, that form **3** apparently via **2**[6] and keep their overall shape even upon further reaction to give back **1** or **4** and **5**, show that we do not see topotactic single crystal to single crystal reactions but controlled crystal disintegrations without detachment of material at outer and inner surfaces (cracks). The calculated crystal densities of **1** are 1.060 and of **3** 1.195 g cm^{-3}, which represents an increase of 13%. The resulting strain is certainly not fully

developed as we have a mixture of **1** with **3** in the surface region of the single crystal. The strain is relieved but slowly if oxygen is excluded {only a few sporadic cracks in the [100] direction of the original crystal; not seen in Fig. 2 (left)} and it takes a long time to form the increased features of the Figs 5 and 2 (left) by the reverse thermal reaction.

Conversely, the strain is released by crack formation if oxygen had formed the additional products **4** and **5**, as can be seen in the early stages by AFM and later after the reverse reaction on the surface by ordinary light microscopy (Figs 2, 5 and 6). It is essential for these results that the reacted surface material does not detach after the phase rebuilding [e.g. Fig. 5(b) and (c)] and phase transformation steps [e.g. Fig. 5(d) and (e)]. Otherwise, the thermal transformation of **1** into **3** could be complete, although **3** would revert into **1** at room temperature.

The molecular packing of **1** exhibits interlocked monolayer sheets of molecules of **1** with one methyl group and five aromatic hydrogen atoms per molecule pointing outward on either side. That feature is most easily visualized with a large section of the crystal (four stacks along *a*, three along *c* and three along *b*, the latter hidden behind the front molecules). The (001) cleavage planes are seen at the (long) *a*-axes of the unit cell in Fig. 7. These cannot, of course, be used on the (001) face. That feature fits very well with the AFM results: owing to the interlocking we obtain no trenches initially [such trenches would be expected on the non-occurring (010) face] but only at the end of the reaction when the reacted crystal relaxes. The first cracks on (001) (cleavage plane) appear in the [010] direction (Fig. 5), but that finding cannot be derived from the initial lattice of **1**. A second feature is the involvement of layers on (001) particularly in Fig. 5(b), that gives a good impression of how they help in having the molecules move from the surface roughness to form a very smooth flat crystal surface. Importantly, it is easier to generate cracks on (100) along [010], as the cleavage planes end there. The (nearly) orthogonal cracks that follow later cannot be derived from the original lattice as they occur after completion of long-range molecular movements that are evident from the flattening of the very high (although submicroscopic) roughness in Figs 5 and 6 as detected by AFM.

Molecular mechanism. The interpretation of the molecular mechanism has to take into account the enormous geometric changes in the crystal confinement. The lack of melt phases is confirmed by the DSC results (that have exotherms well above the reaction temperature) and the very distinct AFM images. The possibilities for internal rotation and twist in crystals have been investigated in detail,[2,8] whereas the structures and mechanistic details for **1** → **2** → **3** have been exhaustively investigated for the solution reaction.[6] It does not appear that these processes may occur in the solid bulk. In particular, it is not possible to envisage an internal rotation step as formulated in Scheme 1 within the crystal of **1**: rotation around the central bond in the fixed lattice by as little as +10° or −10° leads to severe van der Waals interactions (e.g. 64% of the standard distance). These become unsurmountable at 20° rotation (e.g. 39% of C/H, 43% of H/H and 50% of C/C standard distances). Fortunately, both the AFM and microscopic images and the variation in yield in relation to the crystal size point to mere surface reactions both at the rough outer surface and at cracks that may be present inside the crystal. That is, the internal rotations occur only outside the confinement of the crystal and a significant conversion is possible by the long-range molecular movements with formation of characteristic surface structures if **3** is formed. A similar problem exists for the reverse reaction of **3** to **1**. Again it occurs only outside the crystal confinement. At room temperature it does not easily penetrate into the previously formed new phase. Thus, the green color survives for several days (shorter in the presence of oxygen) and that is true even at elevated temperatures of 40–50 °C. Importantly, the crystal photos (Fig. 2) indicate that the green that was formed at certain spots inside the crystal survives for several weeks as there is a higher confinement. Most importantly, the surface dependence of the yield of **3** (no increase with micronized powder but about double the yield with ground material in KBr) supports well what the careful look at the images indicates.

CONCLUSIONS

The presumed single crystal to single crystal transformation of the thermochromic system **1/3** could not be verified by close scrutiny with AFM, microscopy and yield determinations. The fact that sharp crystal edges are only slightly modified is insufficient evidence for a topotactic conversion. Clearly, a surface reaction that produced a very deep green color and significant transformation due to long-range molecular movements (phase rebuilding and phase transformation[2] as guided by the crystal packing) and the lack of detachment of reacted material hid the fact that nothing occurred under the surface region in the bulk except at internal cracks. A 1 μm high roughness and more was levelled or created on the crystals of **1** upon the thermal reaction. However, the yield of **3** was considerably larger than what might be derived from a 1 μm layer on the single crystal. Therefore, it is important to note that microscopic images of thermochromic crystals and even AFM measurements on those crystals (the same applies to photochromic crystals) may give an incomplete analysis and require further tests with regard to yields and their dependence on the grain size. The puzzle of internal rotation around a single bond within the crystal lattice that could not be modelled owing to unsurmountable interactions was

resolved: the forward and backward reactions occur only at the surface in this particular case even though considerable conversion is observed.

EXPERIMENTAL

IR spectra were measured with a Perkin-Elmer 1720-X FT-IR spectrometer and ^{1}H NMR spectra with a Bruker WP300 spectrometer. AFM measurements were made with a NanoScope II; all AFM surface data are given in fully interactive VRML files at the epoc website at http://www.wiley.com/epoc.

Compound **1** was prepared as described previously[3] and recrystallized from acetone. Single crystals of **1** having approximate dimensions of 3.2, 1.3 and 0.5–1 mm were glued to a magnetic support for easy mounting on the AFM head. The AFM procedure and imaging details have been described elsewhere.[2] After measuring the untreated crystal, the sample was heated in a vacuum or in ambient air to 140–145 °C and probed after the specified times, after remounting as close as possible to the initial site where a change in the angle of measurement might have been necessary for an optimized image, owing to the particularly strong changes in the topographies.

Microscopic inspection and photography were performed on a standard Zeiss microscope at 100-fold enlargement with illumination from above. Anaerobic manipulations were performed in a glove-box under 99.998% argon. The ball-mill technique has been described elsewhere.[2] A Teflon beaker and Teflon balls were used for micronizing **1** down to largely adhering particles about 1 μm in size.

X-ray analysis. *Data collection.* A colorless prismatic crystal of **1** ($C_{42}H_{38}$) having approximate dimensions of $0.34 \times 0.20 \times 0.16$ mm was mounted on a glass fiber. All measurements were made on a Rigaku AFC7R diffractometer with graphite monochromated Mo Kα radiation and a rotating anode generator.

Cell constants and an orientation matrix for data collection, obtained from a least-squares refinement using the setting angles of 25 carefully centered reflections in the range $23.89 < 2\theta < 28.48°$, corresponded to a C-centered monoclinic cell with dimensions $a = 24.425(3)$ Å, $b = 7.431(2)$ Å, $c = 9.456(2)$ Å, $\beta = 98.50(2)°$, $V = 1697.6(7)$ Å^3. For $Z = 2$ and $FW = 542.76$, the calculated density is 1.062 g cm^{-3}. Based on the systematic absences of hkl ($h + k \neq 2n$) packing considerations, a statistical analysis of intensity distribution and the successful solution and refinement of the structure, the space group was determined to be $C2$ (No. 5). The data were collected at a temperature of 23 ± 1 °C using the $\omega - 2\theta$ scan technique to a maximum 2θ value of 55.0°. Omega scans of several intense reflections, made prior to data collection, had an average width at half-height of 0.42° with a take-off angle of 6.0°. Scans of $(1.57 + 0.30\tan\theta)°$ were made at a speed of 16.0° min^{-1} (in omega). The weak reflections [$1 < 10.0\sigma(I)$] were rescanned (maximum of five scans) and the counts were accumulated to ensure good counting statistics. Stationary background counts were recorded on each side of the reflection. The ratio of peak counting time to background counting time was 2:1. The diameter of the incident beam collimator was 1.0 mm and the crystal to detector distance was 235 mm. The computer-controlled slits were set to 3.0 mm (horizontal) and 3.0 mm (vertical).

Data reduction. Of the 2412 reflections which were collected, 2113 were unique ($R_{int} = 0.011$). The intensities of three representative reflections were measured after every 150 reflections. No decay correction was applied.

The linear absorption coefficient, μ, for Mo Kα radiation is 0.6 cm^{-1}. An empirical absorption correction based on azimuthal scans of several reflections was applied which resulted in transmission factors ranging from 0.96 to 0.99. The data were corrected for Lorentz and polarization effects. A correction for secondary extinction was applied (coefficient = 2.05915×10^{-6}).

The structure was solved by direct methods[9] and expanded using Fourier techniques.[10] The non-hydrogen atoms were refined anisotropically. Hydrogen atoms were included but not refined. The final cycle of full-matrix least-squares refinement was based on 2303 observed reflections (all data) and 191 variable parameters and converged with unweighted and weighted agreement factors of $R(F) = 0.0375$ for observed data [$I > 2\sigma(I)$] and $wR(F^2) = 0.1080$ for all data. All calculations were carried out using the teXsan crystallographic software package[11] (CCDC 159144).

Epoc material

The supplementary material available at the epoc website at http://www.wiley.com/epoc contains the crystal structure details of **1** in CIF format together with the structure factors as well as the color images in GIF format and interactively usable full original 3D data of the images in VRML format in high and low resolution in order to allow for critical evaluation of the AFM results, their analytical use with suitable imaging software and future data mining. Interactive viewing is possible with public domain software, e.g. Cosmo Player or Blaxxun via Internet Explorer.

REFERENCES

1. Nakanishi H, Jones W, Thomas JM, Hursthouse MB, Motevalli M. *J. Phys. Chem.* 1981; **85**: 3636–3642; *J. Chem. Soc., Chem. Commun.* 1980; 611–612; Nakanishi H, Jones W, Thomas JM. *Chem. Phys. Lett.* 1980; **71**: 44–48; Kaupp G. *Adv. Photochem.* 1995; **19**: 149–177.

2. Kaupp G. In *Comprehensive Supramolecular Chemistry*, vol. 8, Davies JED (ed). Elsevier: Oxford, 1996; 381–423.
3. Toda F, Ohi M. *J. Chem. Soc., Chem. Commun.* 1975; 506.
4. Toda F, Garratt P. *Chem. Rev.* 1992; **92**: 1685–1707.
5. Toda F. *Eur. J. Org. Chem.* 2000; 1377–1386.
6. Boese R, Benet-Buchholz J, Stanger A, Tanaka K, Toda F. *Chem. Commun.* 1999; 319–320.
7. Toda F, Dan N, Tanaka K, Takehira Y. *J. Am. Chem. Soc.* 1977; **99**: 4529–4530.
8. Kaupp G, Haak M. *Angew. Chem., Int. Ed. Engl.* 1996; **35**: 2774–2777; Kaupp G, Schmeyers J. http://www.photobiology.com/photobiology99/contrib/kaupp/; *J. Photochem. Photobiol. B.* 2001; **59**: 15–19.
9. Altomare A, Burla MC, Camalli M, Cascarano M, Giacovazzo C, Guagliardi A, Polidori G *J. Appl. Crystallogr.* 1994; **27**: 435.
10. Beurskens PT, Admiraal G, Beurskens G, Bosman WP, de Gelder R, Israel R, Smits JMM The DIRDIF-94 Program System. Technical Report of the Crystallography Laboratory, University of Nijmegen: Nijmegen, 1994.
11. teXsan: Crystal Structure Analysis Package. Molecular Structure Corporation, The Woodlands, USA, 1985, 1992.

